Forward Looking Analysis Approach to Assess Copper Acetate Thermal Decomposition Reaction Mechanism

Itab Youssef, Sécou Sall, Thierry Dintzer, Sana Labidi* 🔾**, Corinne Petit**

Institut de Chimie et Procédés pour l'Energie, l'Environnement et la Santé, Université de Strasbourg, UMR7515 CNRS, 25 rue Becquerel, Strasbourg, France
Email: alkheder@unistra.fr, ssall@unistra.fr, thierry.dintzer@unistra.fr, *slabidi@unistra.fr, corinne.petit@unistra.fr

Abstract

Thermal decomposition course of copper acetate monohydrate was monitored by combining diffuse reflectance infrared Fourier transform spectroscopy (DRIFT) coupled with μ gas chromatography-mass spectrometry (μGC-MS) with other analytical techniques (thermogravimetry analysis and *in situ* X-ray diffraction). Non-isothermal kinetic was examined in air and Ar. A complete analysis of the evolution of infrared spectra matched with crystalline phase transition data during the course of reaction allows access to significant and accurate information about molecular dynamics. While thermogravimetry gives broad conclusion about two steps reaction (dehydration and decarboxylation), in line approach (*in situ* X-ray and *in situ* DRIFT coupled to μGC-MS) is proposed as an example of a new robust and forward-looking analysis. While decomposition mechanism of copper acetate monohydrate is still not well elucidated yet previously, the present in-line characterization results lead to accurate data making the corresponding mechanism explicit.

Keywords

In-Operando Spectroscopy and Chromatography, Thermal Decomposition Reaction Mechanism, Copper Acetate, Cross-Linked Characterization Data

1. Introduction

Continuous reaction and analysis is a relevant approach for sustainable chemical process [1] [2]. Ideally, techniques should provide scalable data and should be suitable for adaptation to industrial equipment (for ultimate application to process and quality control). One of the main current challenges is to design

noninvasive techniques able to analyze data about different reaction media: powder, solid, liquid and gases. Two strategies could be proposed: continuous sampling coupled with fast analytical technique on one hand and *in situ* spectroscopic analysis on the other hand. Both approaches are complementary.

Metal carboxylates are useful reagents particularly for organic synthesis [3] and applied in several fields of research as solid-state, surface chemistry and catalysis [3] [4] [5] [6]. The thermal decomposition of metal carboxylates is a feasible route to synthesize metal nanoparticles suitable for catalytic purposes [7] [8] with specific properties based on carboxylates species. This reaction pathway concerning reaction media and applied conditions tailor final products yield, selectivity and chemical structure. Thermal dehydration and decomposition of metal acetate have been studied broadly under various conditions [5] [9] [10]. Copper is an interesting metal according to its properties and environmental applications. For example, Cu or CuO nanoparticles are effective to remedy a range of bacterial pathogens involved in hospital-acquired infections [9]. Some green paintings are based on copper derivatives [11] as copper acetate, silicates, $Cu(Ac)_2 \cdot H_2O$ has a simple process under heating, one step of dehydration followed by a step of decomposition giving rise to Cu_xO_y species as presented by Mansour [5]. Thermal gravimetric analysis (TGA) was a common tool for those studies and was used by some researchers to suggest the obtained copper oxides. Other researchers proposed intermediates species as Z. Lin *et al.* [12] with the formation of $CuAc_2$ peroxides. Despite intensive studies of copper carboxylates structures, no clear mechanism had been hold to illustrate thermal decomposition of these precursors. Different mechanisms for copper acetate monohydrate thermal decomposition were proposed by several authors with some disagree with each other [5] [12] [13]. Proposal of those mechanisms was based on solid material state identification only. Several techniques are conventionally added to thermogravimetry analysis (TGA) for monitoring metal carboxylates species, coupling with differential scanning calorimetry (DSC) or additional analysis of samples with X-ray diffraction (XRD), electronic microscopies or infrared (IR) [5] [12] [14]. Each technique provides specific information of gas or solid species. Moreover, developing new process based on miniaturization and coupled analysis technique made reaction study cost-effective and intensified. To obtain decomposition and reaction mechanism, single characterization technique alone could not be enough. Recently, diffuse reflectance infrared Fourier transform spectroscopy (DRIFTS) with an environmental reaction chamber was used by A. Kaftan *et al.* [15] to elucidate reaction mechanisms for water gas shift and methanol steam reforming. The present work deals with the development of *in-situ* analytical approach for thermal decomposition study of copper acetate precursor in miniaturized DRIFT chamber coupled to μ gas chromatography and mass spectrometry (μGC-MS). This original coupling with new analytical approach has been developed in the lab to produce a large number of data characteristic for gas and solid species in the same time and temperature. In this article, *in-situ*

XRD and TGA analysis were matched with *in-situ* DRIFT coupled to μGC-MS to identify both reagents by one hand and solid and gas products by the other hand for thermal mechanism reaction. The original coupling detailed by the present work allows accessibility for accurate data about mechanism steps. This work reports in-line characterization of copper acetate monohydrate thermal decomposition as a potential example for mechanism proposal by the coupling of in-line techniques. Our article will appeal for researchers having focus on development of analytical techniques but also of solid chemistry and catalysis. It deals with an example of thermal decomposition reaction to present an optimal cross of multiple *in-situ* characterization results to discuss mechanism reaction with more accurate data. Mechanism understanding is crucial to control material structure, thermodynamic phase stability and synthesis process. By the present work, thermal decomposition of $Cu(Ac)_2 \cdot H_2O$ is used as an example to demonstrate that a simple profile of TGA correspond to complex phenomena at molecular scale detectable by coupled techniques.

2. Experimental

2.1. Materials

The commercial crystalline copper (II) acetate mono-hydrate $Cu(Ac)_2 \cdot H_2O$ ($Ac = CH_3COO$) was an ACS product of reagent grade (>98%) and used without further purification.

2.2. Apparatus

The thermal decompositions of copper acetate were analyzed by various follow-up techniques: *in-situ* X-ray diffraction (XRD), thermogravimetry analysis (TGA), *in-situ* diffuse reflectance infrared Fourier transform spectroscopy (DRIFT) coupled to micro gas chromatography (μGC) and mass spectroscopy (MS).

2.3. Methods

2.3.1. Thermal Analysis

The X-ray diffraction of copper acetate monohydrate was performed using TUR-M62 diffractometer with copper anticathode ($\lambda = 1.54$ Å), 34 kV voltage and 25 mA current. The XRD patterns were acquired for 2θ angles ranging from 10° to 70°, with 0.03° steps. The XRD measurements were conducted in temperature programmed mode. For this purpose, Bruker D8 Advance diffractometer equipped with temperature programmed chamber was used. The XRD patterns were collected at temperatures ranging from 30°C to 400°C with heating rate of 10°C/min flowing air or Ar. After the heating, the solid decomposition products were analyzed at room temperature into the chamber. Corresponding diffractograms during the acetate decomposition were collected at 30°C, 110°C, 170°C, 190°C, 250°C and 370°C. Thermal decomposition of sample was carried out in a TGA thermogravimetry (series Q5000) of TA Instruments in a flowing air or argon atmosphere (10 ml·min^{-1}). Approximately, 2 - 3 mg of sample was heated

in an open platinum crucible at a rate of 15˚C/min up to 400˚C, incorporating a controlled rate thermal analysis program. To confirm the feasibility of comparing sample results by different techniques, TGA of $Cu(Ac)_2·H_2O$ and $Cu(Ac)_2·H_2O$ in KBr were tested and gave almost the same result for the same temperatures.

2.3.2. *In Situ* DRIFT-GC and MS Coupled Measurements

The *in-situ* experiments have been performed in a Vertex 70 Bruker IR spectrometer equipped with a one-pot sample compartment. The *in situ* setup provides all necessary gas in and outlets for flow control and allows temperature measurements. Mass flows were regulated using mass flow controllers (Bronkhorst). For DRIFTS, we used a controlled temperature reaction home-made chamber (7 ml), smaller than high-temperature chamber from Harrick, fitted with ZnSe windows and a Praying Mantis diffuse reflection accessory (Harrick). Temperatures were directly measured in the center of the catalytic bed by mean of a 0.75 mm * 150 mm type K thermo-couple. The apparatus originality is due to its coupling mode: it is an IR spectrometer coupled with a mass spectrometer and gas phase chromatograph (μGC-MS). This allows measurements *in situ* during a reaction under controlled atmosphere. The flow of gas is recovered at the outlet of the chamber and is brought to through a transfer rod to the μGC-MS switchgear. The experiments are performed by a new coupled instrumentation obtained by miniaturized cell, a DRIFT spectroscopy, 3 micro gas chromatographs and a mass spectrometer. One of the present technique advantages is to allow data acquisition throughout the transformation on the solid material and on the produced gases simultaneously. The coupling with gas chromatography (gas molecule identification by mass spectrometry) makes possible to monitor continuously the emission of gas. These experimental steps are systematically carried out during the sample preparation for DRIFTS analysis. The QMS data shown here were corrected by the following m/z values obtained by calibration: CO_2 gas (m/z = 44), H_2O (m/z = 18), acetic acid (m/z = 60) and acetone (m/z = 43). The spectra are measured from 600 to 4000 cm^{-1} with a resolution of 4 cm^{-1} (15 spectra/second) and are directly collected by the computer. The reaction chamber is equipped with ZnSe windows and a gas flow of 10 $cm^3·min^{-1}$ across the sample. The experiments are carried out from room temperature to 600˚C ($15˚C·min^{-1}$), to avoid heating during high temperature studies, the chamber is equipped with a cooled double wall of water flow to control temperature. Samples are prepared by dilution (10 wt%) with dry powder of potassium bromide (KBr) or zinc selenide (ZnSe) as a diluent. Different conditions of test are made to show the influence of the presence of water interaction with the diluent during the decomposition steps. Powders are milled together and then placed on the sample holder in the chamber. This cell is closed and purged with helium (10 mL/min) for 5 minutes, sufficient time to purge the small chamber. The desired gas is then introduced, with a purge of 5 minutes for each experimental conditions variation. All gases were used without further purification (He:Alphagaz

2, >99.9999%; Ar:Alphagaz 2, >99.9999%; synthetic air Air Products, >99.9999%). No reabsorption, especially water, has been observed by leaving KBr sample overnight under flow.

3. Results

3.1. Study of Copper Acetate Decomposition by XRD and TGA

In situ XRD profiles of $Cu(Ac)_2 \cdot H_2O$ under heat treatment at 30˚C, 110˚C, 170˚C, 190˚C, 250˚C and 370˚C are showed by **Figure 1**. Copper acetate monohydrate and copper acetate are both observed in the XRD profiles at room temperature and mainly $Cu(Ac)_2$ at 110˚C under air and Ar. The decomposition of acetate species starts at 190˚C and finishes before 250˚C as shown by the acetate cristal disappearing on the XRD profile at 250˚C under air and at 190˚C under Ar. This compound, in opposition to other acetate as $Co(Ac)_2 \cdot 4H_2O$ [16], do not melted during the dehydration step. Between 190˚C and 250˚C, broad peaks appear in the range of 35˚ - 40˚ of 2θ. These profiles should correspond to intermediate species since copper oxides and copper are detected in XRD profiles further. According to heat treatment media, different oxides appear above 190˚C. Cu_2O and CuO appear at 250˚C and 370˚C respectively under air. Whereas, these both oxides appear simultaneously under Ar and get transformed to Cu around 370˚C.

TGA/TGD curves of $Cu(Ac)_2 \cdot H_2O$ are shown in **Figure 2**. These studies confirm the two steps as presented mainly in the literature [5] [9] [12], one first step for dehydration then decarboxylation with differences according to heat media. The curves of copper acetate monohydrate decomposition obtained by TGA/DTG (**Figure 2**) display mainly two mass loss steps in the temperature range from 22˚C to 400˚C, and one mass gain step in air. The corresponding data of mass changes are listed in **Table 1**. The listed experimental values of first mass loss step agree with theoretical value (9.0%) of absolute dehydration of $Cu(Ac)_2 \cdot H_2O$ under air and Ar. The second mass loss step was commonly attributed
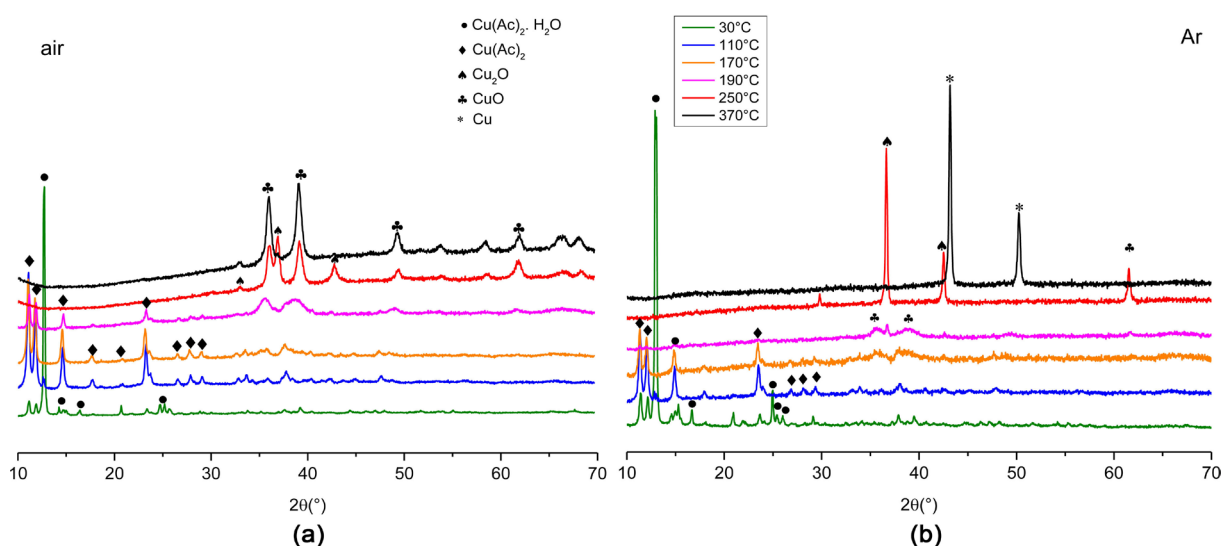
Figure 1. XRD patterns for copper acetate monohydrate thermal decomposition under air and Ar.
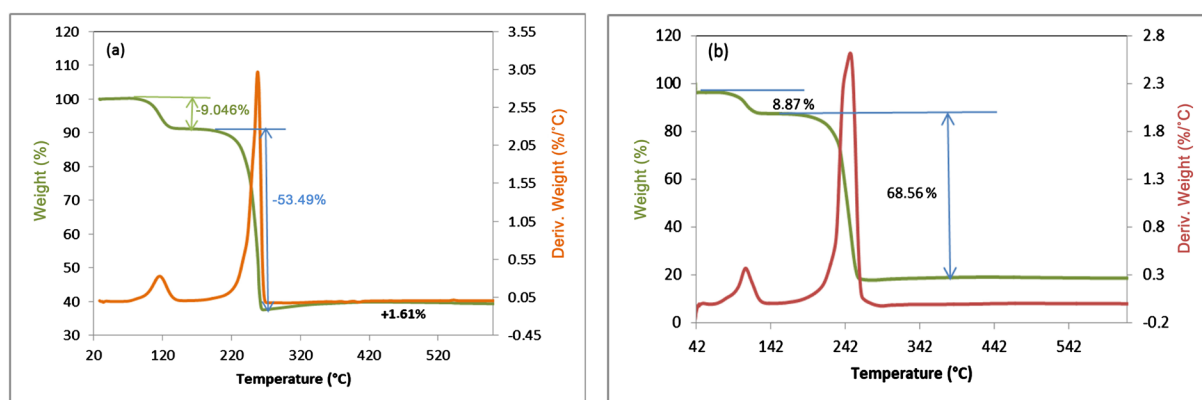
Figure 2. TGA and DTG curves for thermal decomposition of $Cu(Ac)_2 \cdot H_2O$ in air (a), in Ar (b).

Table 1. Mass changes of $Cu(Ac)_2 \cdot H_2O$ thermal decomposition under air and Ar.

Step		Temperature range (°C)	Mass change (%)	Theoretical mass change (%)
	1	100 - 170	−9.0	−9.0
Air	2	230 - 310	−53.5	−55.1
	3	310 - 600	+ 1.6	+4
Ar	1	80 - 140	−8.9	−9.0
	2	200 - 275	−68.6	−65.3

to $Cu(Ac)_2$ decomposition since the experimental value of mass loss under air for this step is consistent with the theoretical one (−55.1%) [17]. The mass increase between 310 and 600°C is lower than theoretical value (4%). Cu_2O is only partially oxidized to CuO at 600°C. According to XRD patterns, $Cu(Ac)_2$ decomposition under Ar between 195°C and 275°C produce Cu_2O and CuO which are reduced thereafter to Cu since the experimental value of the mass loss for steps was quite close to the theory value. Difference between theoretical and experimental values of mass gain under Ar could be explained by multi-crystal phase formation during heat treatment between 230°C and 310°C. TGA seems to propose a relative simple phenomena for the degradation of $Cu(Ac)_2 \cdot H_2O$ but do not explain reaction mechanism. Thus, solid and emitted gases must be analyzed simultaneously *in situ* to identify intermediate species and then elucidate $Cu(Ac)_2 \cdot H_2O$ thermal decomposition mechanism. According to TGA and XRD *in situ* results, $Cu(Ac)_2 \cdot H_2O$ thermal decomposition reaction could be given broadly as follow without consideration of organic moieties because of lack of corresponding data:

1) $Cu(CH_3COO)_2 \cdot H_2O \rightarrow CuO$ under air;
2) $Cu(CH_3COO)_2 \cdot H_2O \rightarrow Cu$ under Ar.

3.2. Analysis of Overall DRIFT Spectra Evolution during Copper Acetate Decomposition: Relation between Reaction Course and Modifications at the Molecular Scale

In this study, DRIFT analysis monitor phenomena occurring at the molecular

scale during thermal decomposition reaction. To achieve this goal, main spectral regions were identified then we focused on a limited number of spectra for Cu(Ac)$_2$·H$_2$O decomposition at specific temperature. The *in situ* DRIFT spectra of Cu(Ac)$_2$·H$_2$O from room temperature to 410°C in air and in He, are showed in **Figure 3**, and peaks assignment are listed in **Table 2** in agreement with Z. Lin and Mathey [12] [14].

3.2.1. Dehydration Step and Water Influence on DRIFT Spectra

As shown in **Figure 4**, absorptive peak of O-H bond of water (3380 cm^{-1}) and free O-H (3585 cm^{-1}) distinctly weaken from 100°C approximately (beginning of H$_2$O desorption from precursor solid surface) and corresponds to the dehydration of Cu(Ac)$_2$·H$_2$O. The results from the DRIFT spectra complete the TGA/DTG results and show slower leaving of OH moieties under air than under inert gas. The small amount of water staying on copper is able to change the mechanism of acetate decomposition and this issue will be discussed later.

3.2.2. Decarboxylation/Decomposition Step

DRIFT domain spectrum between 1150 and 1850 cm^{-1} contained characteristic peak of bidentate/bridged copper acetate bonds vibration mainly. During decomposition course, we observed intensity variation and shift position of peak intensities in that spectra region (**Figure 5**). Consistent with other references in literature [18] [19] [20] [21], DRIFT bands are observed for copper acetate dehydrate at 1608, 1580, 1441, and 1362 cm^{-1}. The carboxylate symmetric stretch is located as two bands at 1441 and 1362 cm^{-1}, while the asymmetric one is observed at 1608 and 1580 cm^{-1}. Intensities of listed peaks are influenced by temperature variation according to moisture level on the substrate and configuration of organic moieties. Above 200°C under air and Ar, bands of asymmetric stretching acetate at 1608 are cleaved to main bands at 1620 and 1580 cm^{-1} according to bidentate-monodentate transformation [22] (**Figure 5**). The diffractograms
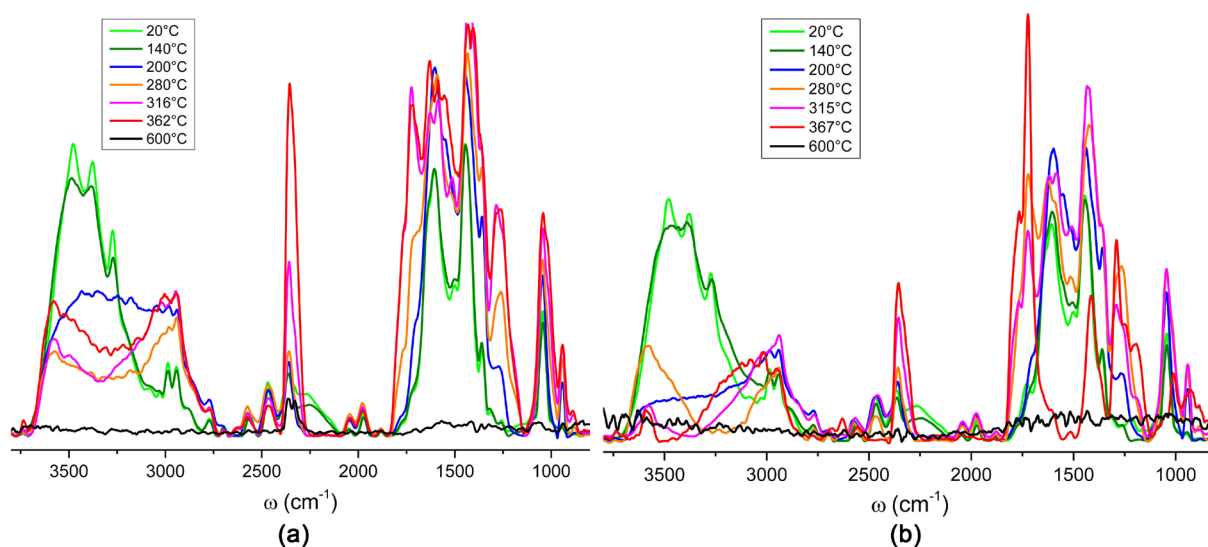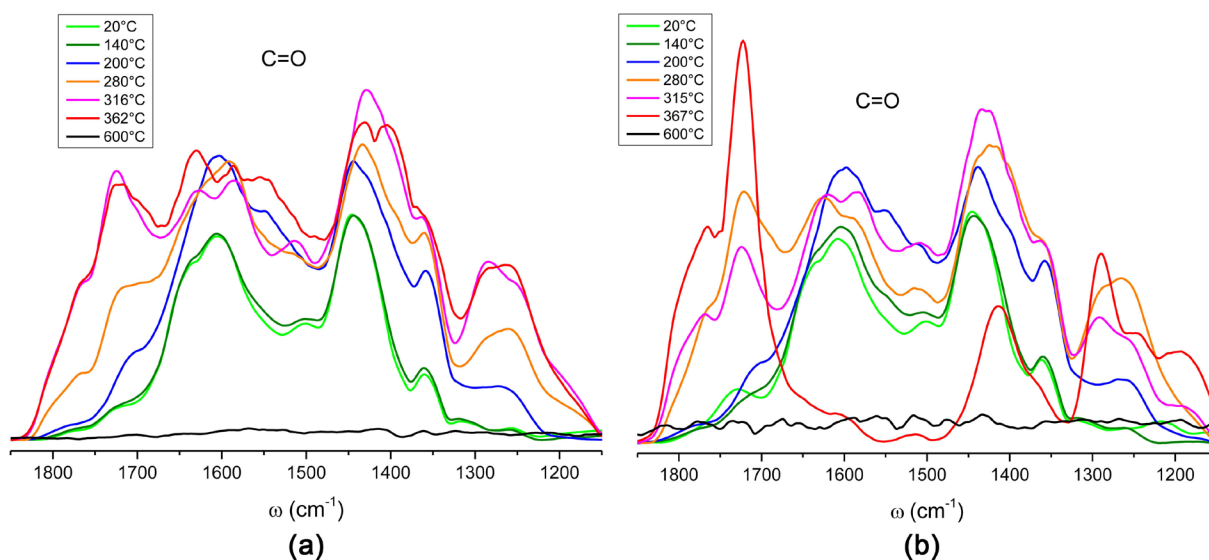

Figure 3. *In situ* DRIFT of Cu(Ac)$_2$·H$_2$O in KBr under air (a) and Ar (b) between 4000 and 800 cm^{-1}.

Table 2. Assignments of DRIFT spectra of $Cu(Ac)_2 \cdot H_2O$.

Wavenumber (cm^{-1})	Assignment
3585	O–H stretching in acetic acid/CO_2 gas
3478 - 3373	O–H stretching in water
3000 [18]	CH_3 asymmetric stretch in acetone
2989, 2942	C–H stretching in methyl
2360	CO_2 gas
1715 [19]	C=O stretching in acetone
1722 [20]	C=O stretching in acetic acid
1608	C=O asymmetric stretching
1620	O-H in H_2O,
1613 [21]	Cu–H stretching in CH_3-CuH^-
1580 - 1550	C=O asymmetric stretching
1573 [20]	O-H stretching in chemisorbed H_2O
1450 - 1430	C=O symmetric stretching
1375 (1362) [20]	C=O symmetric stretching
1355	C–H bending in methyl
1243 [20]	C-OH stretching in acetic acid
1203 [21]	CH_3-Cu, CH_3 deform
1051 - 1033	C–CH framework vibration
944	C–O stretching in acetic acid
1012 [21]	CH_3-CuH, CH_3 deform
668 - 682	CO_2 gas
648 [21]	CH_3-Cu, CH_3 rock
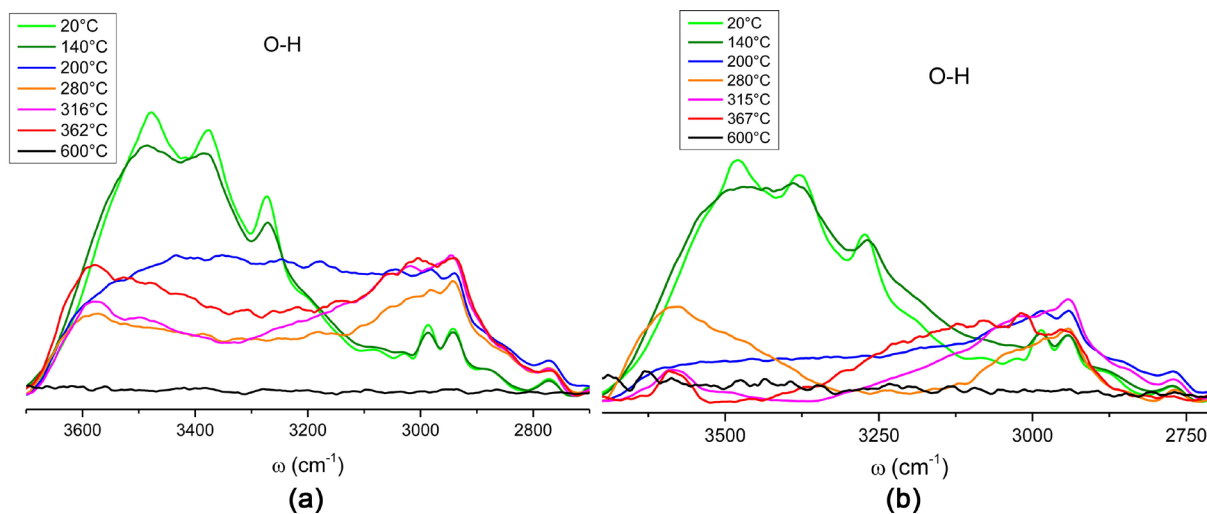
Figure 4. *In situ* DRIFT of $Cu(Ac)_2 \cdot H_2O$ in KBr under air (a) and Ar (b) between 3700 and 2700 cm^{-1}.

Figure 5. *In situ* DRIFT of [1] Cu(Ac)$_2$·H$_2$O in KBr under air (a) and Ar (b) between 1850 and 1150 cm^{-1}.

of hydrated Cu(Ac)$_2$ (Figure 1) is described as bidentate acetate in the range of 35° and 40° between 190°C and 250°C. Mixed with KBr, the bidentate function is sensitive to H$_2$O-Cu bond length and carboxylate ligands are transformed from bidentate to monodentate species. This structure enhances water hooking on the neighborhood of carboxylate [22] at 1573 cm^{-1}, [20]. Dehydration step is quite similar under Ar and air: specific bands of acetate ligands of Cu(Ac)$_2$ at 1608, 1441 and 1362 cm^{-1} increase from 20°C until 280°C under air and 315°C under Ar (Figure 5). Once this step is achieved, new bands at 1722 and 1260 cm^{-1} referring to C=O and C-OH stretch respectively in acetic acid [20] appear under air and Ar similarly. A main difference according heat treatment media is reported during this stage. Absorptive peaks at 1608 and 1442 cm^{-1} maintain rising intensity till 316°C than fall at 600°C under air. For inert gas, the latest bands disappeared between 315°C and 367°C with an increase of stretching bonds of acetic acid until 367°C (Figure 5). This observation reveals that acetate ligands start to decompose earlier under Ar and are converted to adsorbed acetic acid mainly, while, acetate ligands still bonded to copper metallic center during decomposition step under air. With TGA alone, it wasn't possible to prove the latest conclusion to assess differences in reaction mechanism under air and inert gas.

Figure 6 shows variation of peaks intensity referring to C-CH and C-O at 1044 and 942 cm^{-1} [23] respectively. These two bands increase from 20 to 367°C under air than fall by the end of heat treatment. C-CH and C-O bonds decompose earlier under Ar since relative bands turn before 367°C. This observation illustrates that CH$_3$COO$^-$ group bonded to metallic center as acetate ligand is converted to adsorbed acetic acid under Ar (Figure 5) before its complete decomposition after 367°C. CH$_3$COO$^-$ bonds are strengthened within heat treatment at dehydration and decarboxylation stages according to monodentate-bidentate/bridged transition. According to Campbell and Sharrock [24] [25] binuclear metal centers of copper acetate (II) were proposed to explain com-

pound structure according to NMR signal multiplicity. Mononuclear metal centers are bridged to stabilize electronic deficit on Cu metallic center for Cu acetate monohydrate. **Figure 6** stresses this conclusion since carboxylate bonds are strengthened by peaks rise at 1044 and 942 cm^{-1} in the range of 20˚C and 315˚C.

Gaseous products as CO_2, acetic acid, acetone and ethanol are also detected in the infrared chamber. These volatile products have been proposed in literature [5] [13], which is matched with the present results. We coupled DRIFT with μGC-MS to follow dynamic volatile species emission during decomposition reaction. Characteristic species detected by coupled μGC/MS are CO_2 gas (m/z = 44), H_2O (m/z = 18), acetic acid (m/z = 60) and acetone (m/z = 43). Kinetic gas products emission is recorded within temperature increase and reported by **Figure 7**.

According to the quantification by injection pulses (**Figure 8**), the formation of CO_2 corresponds to 88% of amount of carbon from acetate under air and only 15% under inert gas. Both moieties of acetate (CH_3^- and COO^-) were mainly
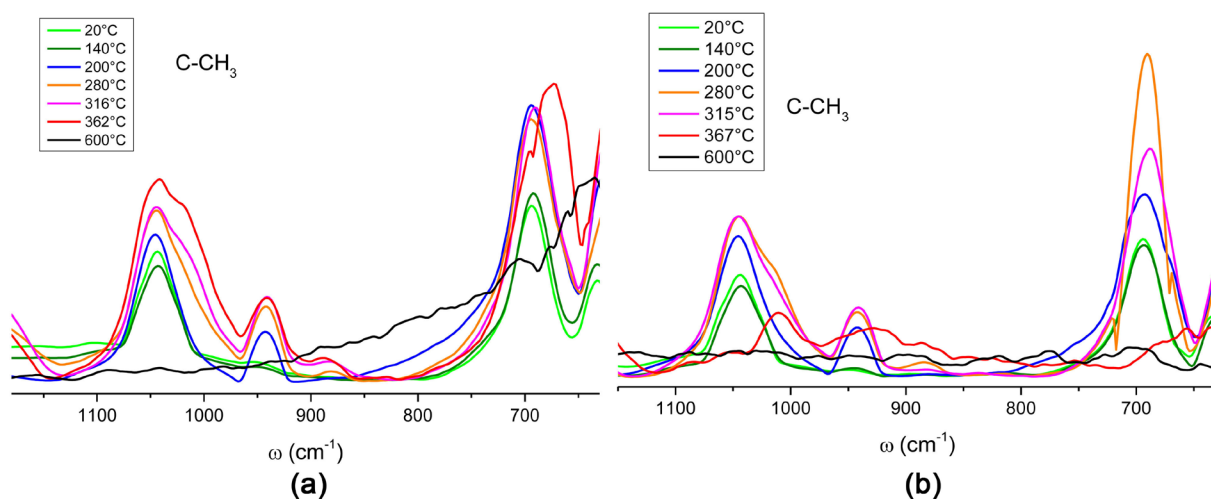
**Figure 6.** *In situ* DRIFT of $Cu(Ac)_2 \cdot H_2O$ in KBr under air (a) and Ar (b) between 1150 and 850 cm^{-1}.
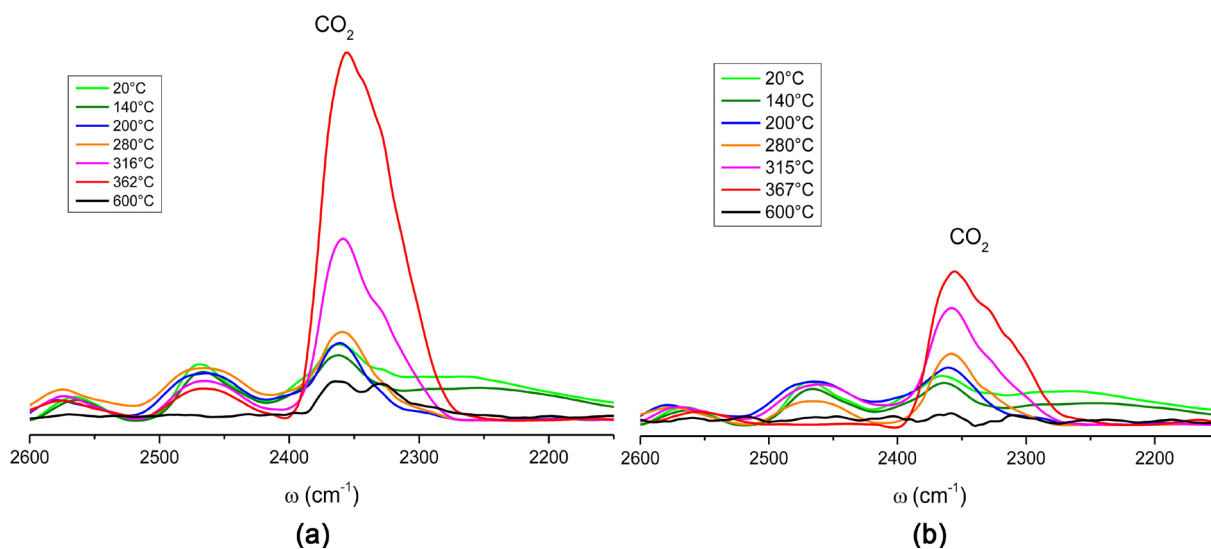
Figure 7. *In situ* DRIFT of $Cu(Ac)_2 \cdot H_2O$ in KBr under air (a) and Ar (b) between 2600 and 2150 cm^{-1}.

oxidized under air but the decomposition of acetate involves the creation of intermediate compounds which is mainly acetic acid under Ar (acetone and ethanol are formed at minor). According to DRIFT (Figure 5) and GC-MS (Figure 7) analysis, $Cu(Ac)_2$ ligands are decomposed in both conditions (air or inert gas) with some similar intermediate species oxidized only under air. The same observation could be made for peak evolution at 2361 cm^{-1} related to vibration modes of CO_2 gas bonds (Figure 8). We examined the intensity of some characteristic peaks within temperature. Figure 9 shows the variation of peaks intensity corresponding to O–H stretching in water, C=O stretching, CO_2 gas and C-CH$_3$ framework vibration mode. This follow-up is used to monitor, within time and temperature, similarly to TGA analysis but with more accurate information than relative mass detection.
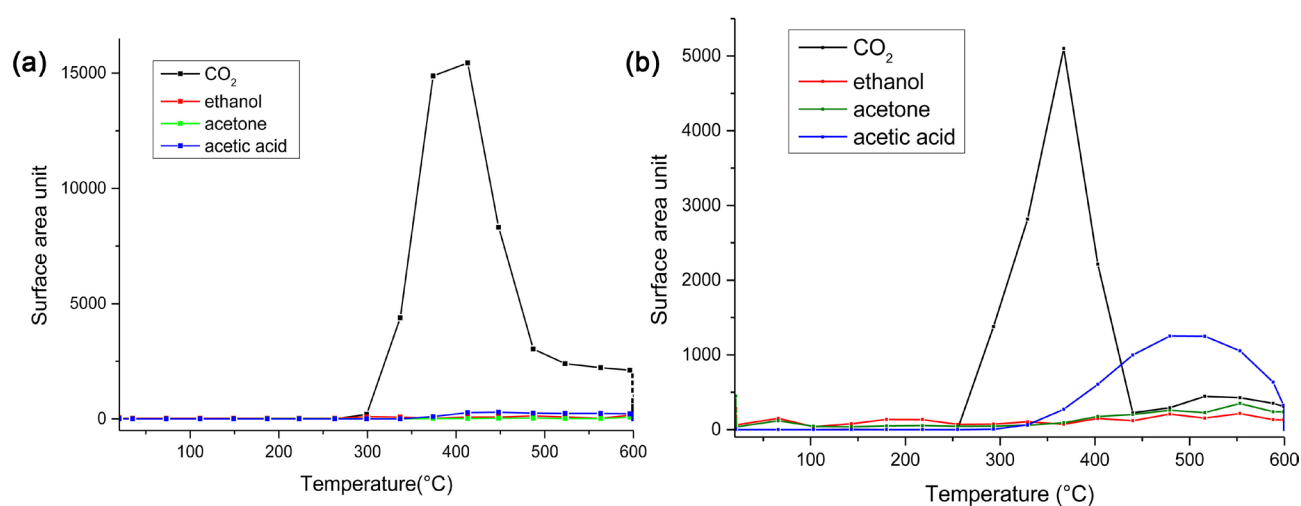
Figure 8. Gas emission quantification by μ GC-MS during $Cu(Ac)_2 \cdot H_2O$ decomposition under air (a) and Ar (b).
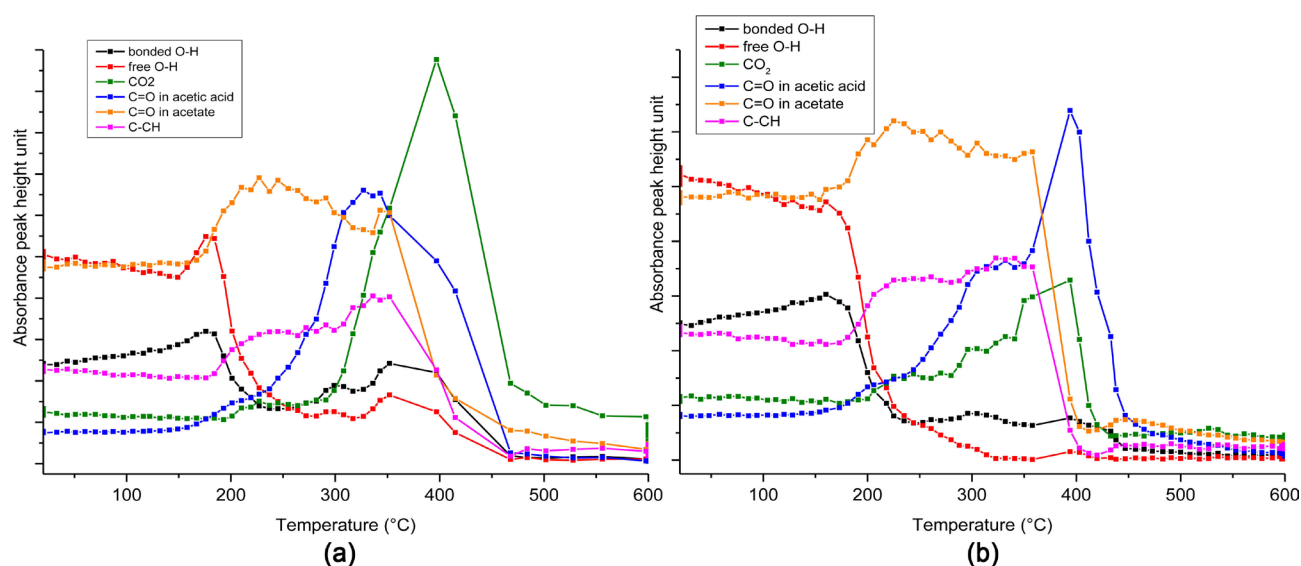
Figure 9. Bands intensities evolution of *in situ* DRIFT spectra within temperature for bonded O-H (3585 cm^{-1}—black), free O–H (3380 cm^{-1}—red), CO_2 gas (2360 cm^{-1}—green), C=O in acetic acid (1722 cm^{-1}—blue), C=O asymmetric (1608 cm^{-1}—orange) and C-CH (1044 cm^{-1}—purple) of $Cu(Ac)_2 \cdot H_2O$ in KBr under air (a) and Ar (b).

4. Discussion

Scheme 1 (in annex section) describes mechanistic dynamic steps during thermal decomposition under air and Ar leading to CuO and Cu respectively as solid with emission of H_2O, CO_2, CH_3COOH, H_2 [26] (according reaction media) and coke deposit [27]. On Scheme 1, structures 1 and 2 describe binuclear complex dehydration step. XRD patterns confirm TGA results concerning dehydration process. H_2O desorption ends at 170°C under air and at 140°C under Ar according to thermal analysis in agreement with XRD patterns (diffractograms pic of copper acetate monohydrate disappeared before 170°C) and DRIFT analysis as shown by Figure 4. Structure transition $1 \rightarrow 2$ could be traduced by the following reaction Equation (1):

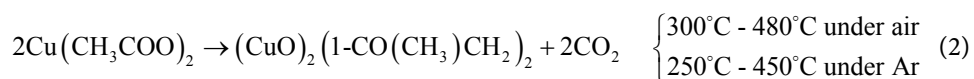$$2Cu\left(CH_3COO\right)_2 \cdot H_2O \rightarrow 2Cu\left(CH_3COO\right)_2 + 2H_2O \quad \begin{cases} 20°C \text{ - } 170°C \text{ under air} \\ 20°C \text{ - } 140°C \text{ under Ar} \end{cases} \quad (1)$$
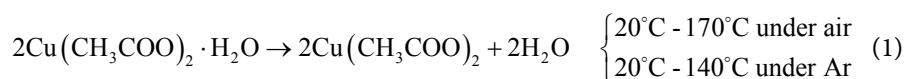
According to TGA data, thermal decomposition of $Cu(Ac)_2 \cdot H_2O$ ends at 310°C under air and 275°C under Ar. Nevertheless, $Cu(Ac)_2 \cdot H_2O$ signal on XRD patterns falls before, in the range of 190°C and 250°C (before 190°C under Ar) with appearance of broad peaks at 2θ ranging from 35° to 40° (Figure 1). Crucially, we observe an increase of C-O stretching bond intensity at 944 cm^{-1} (Figure 6) from 20°C to 310°C approximately then a decrease reaching 600°C. The correlation between the latest observations on TGA, XRD and DRIFT results is worth noting as it concludes on complex transition $2 \rightarrow 3$ (Scheme 1): acetate ligands are shifted from bidentate to monodentate species. Figure 9 confirms this conclusion: C=O bands (1608 and 1718 cm^{-1}) increased within temperature simultaneously with desorption of H_2O moieties (fall of 3380 and 3585 cm^{-1} signal by the end of dehydration steps under Ar and air). Structure 3 is proposed according to H_2O desorption step for carboxylic acid ketonization on acid-base pairs of TiO_2 [28]. H_2O desorption involves C-C coupling between 1-hydroxyl enolate and co-adsorbed acetate to form α-hydroxy γ-carboxy alkoxide. An XRD pattern (Figure 1) confirms Cu_2O lattice formation under air and Ar starts at 190°C - 250°C. Thus, once dehydration step is achieved, Cu_2O network appears ($2 \rightarrow 3$ transition in Scheme 1).

As mentioned by GC-MS data measurements (Figure 7), CO_2 detection on gas phase starts at 300°C under air and 250°C under Ar and reaches maximal values at 413°C and 367°C respectively. Meanwhile, CO_2 is detected on precursor surface from 200°C (both Ar and air). Transition $3 \rightarrow 4$ on Scheme 1 illustrates CO_2 adsorption on cupric center than its desorption for transition $4 \rightarrow 5$. Transition $3 \rightarrow 5$ is resumed by Equation (2) as bellow:

$$2Cu\left(CH_3COO\right)_2 \rightarrow \left(CuO\right)_2\left(1\text{-}CO\left(CH_3\right)CH_2\right)_2 + 2CO_2 \quad \begin{cases} 300°C \text{ - } 480°C \text{ under air} \\ 250°C \text{ - } 450°C \text{ under Ar} \end{cases} \quad (2)$$

Air media promotes complete oxidation of acetate ligands to CO_2 and H_2O (transition $5 \rightarrow 6'$). We note an involving rate of adsorbed acetic acid on Cu_2O (Figure 9(a)) surface under air without its detection by GC-MS. This is ex-

plained adsorbed acetic acid oxidation to CO_2 and H_2O. Indeed, evolution of hydroxyl bands on Figure 4(a) and Figure 9(a) illustrates a signal rise from 280°C to 360°C, which is matching mechanism transition for the final step under air and Cu_2O turns into CuO as latest crystalline phase (fig. a).
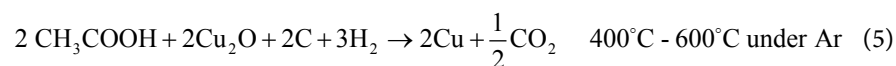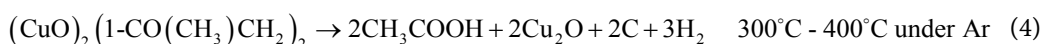
The transition 2 → 3" on Scheme 1 is proposed as one step decomposition of $Cu(Ac)_2 \cdot xH_2O$ (x ≠ 0) to acetic acid and Cu under Ar without CO_2 desorption and copper oxide intermediates. H_2O is essential for this transition that its equilibrium is rather shifted for compound 2.

A notable difference is identified for thermal decomposition under Ar after 300°C compared to the same one under air. Acetic acid is detected by GC-MS (Figure 7(b)) from 340°C and reaches its maximum at 500°C. Its desorption was also predicted by DRIFT spectra (Figure 5(b) and Figure 9(b)) since C=O stretching band at 1722 cm^{-1} increases from 340 until 400°C, thus, CH_3COOH was adsorbed on Cu_2O surface before its desorption. Transition 5 → 9 describe acetic acid desorption. This transition is deeply influenced by water adsorption on copper atoms. Residual H_2O moieties in KBr, since its hygroscopic property, oxidize ligands by nucleophilic substitution. This reaction involves C-O coupling between 1-hydroxyl enolate and coordinated residual H_2O to form *α*-hydroxy alkoxide. The latest intermediate is converted to Cu-CH_3COOH and Cu-CH_3 [28] (Scheme 1. 6 → 9). On Figure 4, OH bands fall are more noticed under Ar rather than under air which confirms the latest hypothesis since H_2O was consumed to form acetic acid. Figure 9(b) stresses this observation: no hydroxyl bands increase after 300°C under Ar contrarily to air. Ligands decomposition under Ar involves Cu_2O phase formation. Copper oxide turns to Cu between 250°C and 370°C with desorption of CO_2 as described by Figure 9(b) plot.

To assess the influence of adsorbed water in mechanism reaction, two types of diluent were tested under Ar: KBr on one hand with hygroscopic property and ZnSe on the other hand. When the diluent is hygroscopic, C=O bands shifted during decomposition process (Figure 5) When the diluent does not interact with water as ZnSe, C=O bands are kept in the same position during heating. Mixed with ZnSe, acetate is bonded to copper as bidentate ligands during dehydration and decomposition steps under air and inert gas. Moreover, gaseous products for $Cu(Ac)_2 \cdot H_2O$ under Ar in ZnSe are different from similar reaction in KBr: GC-MS shows formation of acetone at the same level as acetic acid in addition to CO_2 desorption earlier (annexe?). Acetone formation from acetate heat treatment is described as carboxylic acid ketonization catalyzed by metal oxides reported by several authors [28]. Acetic acid still formed with use of ZnSe which is explained by remained amount of H_2O after dehydration step finished at 170°C as proved by A. Musumeci and co. [10]. Moreover, desorbed products analyzation by TPD with corrected m/e of Ni acetate heat decomposition under He was performed by J.C. De Jesus *et al.* [8] and they confirm H_2O desorption at 162°C than at 373°C with formation of acetic acid and acetone. KBr use leads to acetic acid selectivity so.

Transition $7 \rightarrow 8$ illustrates copper methyl formation ($CuCH_3$) and adsorbed acetic acid after nucleophilic substitution by H_2O. Concerning adsorbed acetic acid, DRIFT spectra shows (**Figure 9(b)**) that its band got intensified from 200°C to 400°C before its decrease within temperature rise under Ar. Simultaneously, acetic acid (as free molecule) is quantified in gas phase by GC-MS from 350°C to 500°C than falls by the end of decomposition reaction (**Scheme 1**, $8 \rightarrow 9$). Cho and co. [21] made infrared characterization of Cu-CH$_3$ and listed 4 main bands at 1612 (Cu-H stretching in CH_3-CuH$^-$), 1203 (CH_3 deform in CH_3-Cu), 1012 (CH_3 deform in CH_3-CuH$^-$) and 648 cm^{-1}. Corresponding bands at 1611, 1198, 1011 and 655 cm^{-1} were identified on DRIFT spectra (**Figure 5(b)** and **Figure 6(b)**) and appeared between 315 and 367°C under Ar. The latest bands are not identified under air (except for band at 655 cm^{-1} which is a large band under air). With increase of heat temperature, Cu-CH$_3$ on Cu_2O bond decomposition could lead to Cu_2O, coke and H_2 or αCHx in general ($8 \rightarrow 9$, **Scheme 1**). At the last step $9 \rightarrow 10$, copper oxide is converted to Cu with emission of CO_2 (re-increase of CO_2 level at 500°C approximately in **Figure 7(b)**).

Last steps of mechanism reaction are resumed by the following reactions equations system (3), (4) and (5) under air and Ar:

$$(CuO)_2 (1\text{-}CO(CH_3)CH_2)_2 \rightarrow 2CuO + 6CO_2 + 5H_2O \quad 370°C \text{ - } 600°C \text{ under air} \quad (3)$$

$$(CuO)_2 (1\text{-}CO(CH_3)CH_2)_2 \rightarrow 2CH_3COOH + 2Cu_2O + 2C + 3H_2 \quad 300°C \text{ - } 400°C \text{ under Ar} \quad (4)$$

$$2\ CH_3COOH + 2Cu_2O + 2C + 3H_2 \rightarrow 2Cu + \frac{1}{2}CO_2 \quad 400°C \text{ - } 600°C \text{ under Ar} \quad (5)$$

5. Conclusion

The present work deals with thermal decomposition of copper acetate monohydrate under air and Ar. A complete analysis of the evolution of infrared spectra matched with crystalline phase transition data allows to underline detailed steps for reaction mechanism. In-line μGC-MS results about chronologic desorption of major gaseous products (H_2O, CO_2 and CH_3COOH) correlate favorably with DRIFT spectra observations and provide accurate information about intermediates structure of copper acetate during heat treatment. While TGA gives broad conclusion about two steps reaction (dehydration and decarboxylation), in line approach (*in situ* X-ray and *in situ* DRIFT coupled to μGC-MS) was used to assess H_2O influence on reaction mechanism under Ar. In fact, H_2O desorption is incomplete during dehydration step as defined by TGA and residual moieties are essential to conclude CH_3COOH acetic acid formation, main gas product under Ar. The present in line approach is proposed as an example of a new robust and forward-looking analysis to highlight crucial information about reaction selectivity, conversion and product structure. This tool could be performed also to predict mechanism path way according to reaction media for a large numbre of products and precursors.

Conflicts of Interest

The authors declare no conflicts of interest regarding the publication of this paper.

References

[1] Scalbert, J., Clemencon, I., Legens, C., Diehl, F., Decottignies, D. and Maury, S. (2015) Development of an Innovative XRD-DRIFTS Prototype Allowing Operando Characterizations during Fischer-Tropsch Synthesis over Cobalt-Based Catalysts under Representative Conditions. *Oil & Gas Science and Technology*, **70**, 419-428. https://doi.org/10.2516/ogst/2014031

[2] Price, G.A., Mallik, D. and Organ, M.G. (2017) Process Analytical Tools for Flow Analysis: A Perspective. *Journal of Flow Chemistry*, **7**, 82. https://doi.org/10.1556/1846.2017.00032

[3] Lin, D.C.K. and Westmore, J.B. (1973) Mass Spectral Studies of Binuclear Metal Complexes: Copper(I) Carboxylates. *Canadian Journal of Chemistry*, **51**, 2999-3005. https://doi.org/10.1139/v73-446

[4] Mansour, S.A.A., Hussein, G.A.M. and Zaki, M.I. (1990) Decomposition of $Cd(CH_3COO)_2 \cdot 2H_2O$ and Creation of Reactive Solid Surfaces—A Spectrothermal Investigation. *Reactivity of Solids*, **8**, 197-208. https://doi.org/10.1016/0168-7336(90)80020-K

[5] Mansour, S.A.A. (1996) Thermoanalytical Investigations of the Decomposition Course of Copper Oxysalts. *Journal of Thermal Analysis*, **46**, 263-274. https://doi.org/10.1007/BF01979966

[6] Brown, M.E., Dollimore, D. and Galwey, A.K. (1980) Reactions in the Solid State. In: Bamford, C.H. and Tipper, C.F.H., Eds., *Comprehensive Chemical Kinetics*, Elsevier, Amsterdam, 134-135.

[7] Trimm, D.L. (1980) Design of Industrial Catalysts. In: Churchill, S.W., Ed., *Chemical Engineering Monograph*s, Elsevier, Amsterdam, 3-36.

[8] Jesus, J.C.D., Gonzalez, I., Quevedo, A. and Puerta, T. (2005) Thermal Decomposition of Nickel Acetate Tetrahydrate: An Integrated Study by TGA, QMS and XPS Techniques. *Journal of Molecular Catalysis A*: *Chemical*, **228**, 283-291. https://doi.org/10.1016/j.molcata.2004.09.065

[9] Ren, G., Hu, D., Cheng, E.W.C., Vargas-Reus, M.A., Reip, P. and Allaker, R.P. (2009) Characterisation of Copper Oxide Nanoparticles for Antimicrobial Applications. *International Journal of Antimicrobial Agents*, **33**, 587-590. https://doi.org/10.1016/j.ijantimicag.2008.12.004

[10] Musumeci, A. and Frost, R.L. (2007) A Spectroscopic and Thermoanalytical Study of the Mineral Hoganite. *Spectrochimica Acta Part A*: *Molecular and Biomolecular Spectroscopy*, **67**, 48-57. https://doi.org/10.1016/j.saa.2006.05.037

[11] Buti, D., Rosi, F., Brunetti, B.G. and Miliani, C. (2013) *In-Situ* Identification of Copper-Based Green Pigments on Paintings and Manuscripts by Reflection FTIR. *Analytical and Bioanalytical Chemistry*, **405**, 2699-2711. https://doi.org/10.1007/s00216-013-6707-6

[12] Lin, Z., Han, D. and Li, S. (2012) Study on Thermal Decomposition of Copper(II) Acetate Monohydrate in Air. *Journal of Thermal Analysis and Calorimetry*, **107**, 471-475. https://doi.org/10.1007/s10973-011-1454-4

[13] Afzal, M., Butt, P.K. and Ahmad, H. (1991) Kinetics of Thermal Decomposition of Metal Acetates. *Journal of Thermal Analysis*, **37**, 1015-1023. https://doi.org/10.1007/BF01932799

[14] Mathey, Y., Greig, D.R. and Shriver, D.F. (1982) Variable-Temperature Raman and Infrared Spectra of the Copper Acetate Dimer $Cu_2(O_2CCH_3)_4(H_2O)_2$ and Its Derivatives. *Inorganic Chemistry*, **21**, 3409-3413. https://doi.org/10.1021/ic00139a028

[15] Kaftan, A., Kusche, M., Laurin, M., Wasserscheid, P. and Libuda, J. (2017) KOH-Promoted Pt/Al_2O_3 Catalysts for Water Gas Shift and Methanol Steam Reforming: An Operando DRIFTS-MS Study. *Applied Catalysis B: Environmental*, **201**, 169-181. https://doi.org/10.1016/j.apcatb.2016.08.016

[16] Wanjun, T. and Donghua, C. (2007) Mechanism of Thermal Decomposition of Cobalt Acetate Tetrahydrate. *Chemical Papers*, **61**, 329-332.

[17] Zhang, K.L., Hong, J.H., Cao, G.H., Zhan, D., Tao, Y.T. and Cong, C.J. (2005) The Kinetics of Thermal Dehydration of Copper(II) Acetate Monohydrate in Air. *Thermochimica Acta*, **437**, 145-149. https://doi.org/10.1016/j.tca.2005.06.038

[18] Hudson, R.L., Gerakines, P.A. and Ferrante, R.F. (2018) IR Spectra and Properties of Solid Acetone, an Interstellar and Cometary Molecule. *Spectrochimica Acta Part A: Molecular and Biomolecular Spectroscopy*, **193**, 33-39. https://doi.org/10.1016/j.saa.2017.11.055

[19] Smith, B.C. (2017) The Carbonyl Group, Part I: Introduction. *Spectroscopy*, **32**, 31-36.

[20] DeCoste, J.B., Peterson, G.W., Schindler, B.J., Killops, K.L., Browe, M.A. and Mahle, J.J. (2013) The Effect of Water Adsorption on the Structure of the Carboxylate Containing Metal-Organic Frameworks Cu-BTC, Mg-MOF-74, and UiO-66. *Journal of Materials Chemistry A*, **1**, 11922-11932. https://doi.org/10.1039/c3ta12497e

[21] Cho, H.G. and Andrews, L. (2011) Infrared Spectra of CH_3-MH, CH_3-M, and CH_3-MH-Prepared *via* Methane Activation by Laser-Ablated Au, Ag, and Cu Atoms. *Dalton Transactions*, **40**, 11115-11124. https://doi.org/10.1039/c0dt01827a

[22] Dudev, T. and Lim, C. (2004) Monodentate versus Bidentate Carboxylate Binding in Magnesium and Calcium Proteins: What Are the Basic Principles? *The Journal of Physical Chemistry B*, **108,** 4546-4557. https://doi.org/10.1021/jp0310347

[23] Mekhemer, G.A.H., Halawy, S.A., Mohamed, M.A. and Zaki, M.I. (2005) Ketonization of Acetic Acid Vapour over Polycrystalline Magnesia: *In Situ* Fourier Transform Infrared Spectroscopy and Kinetic Studies. *Journal of Catalysis*, **230**, 109-122. https://doi.org/10.1016/j.jcat.2004.09.030

[24] Campbell, G.C., Reibenspies, J.H. and Haw, J.F. (1991) Solid-State NMR Studies of Magneto-Structural Correlations in Anhydrous Copper(II) Carboxylates. *Inorganic Chemistry*, **30,** 171-176. https://doi.org/10.1021/ic00002a006

[25] Sharrock, P. and Melnik, M. (1985) Copper(II) Acetates: From Dimer to Monomer. *Canadian Journal of Chemistry*, **63,** 52-56. https://doi.org/10.1139/v85-009

[26] Bellini, J.V., Machado, R., Morelli, M.R. and Kiminami, R.H.G.A. (2002) Thermal, Structural and Morphological Characterisation of Freeze-Dried Copper(II) Acetate Monohydrate and Its Solid Decomposition Products. *Materials Research*, **5**, 453. https://doi.org/10.1590/S1516-14392002000400010

[27] Costa, G., Camus, A. and Marsich, N. (1965) Copper Methoxides Formed by Thermal Decomposition of Copper Methyl in Methanol. *Journal of Inorganic and Nuclear Chemistry*, **27**, 281-285. https://doi.org/10.1016/0022-1902(65)80339-6

[28] Wang, S. and Iglesia, E. (2017) Experimental and Theoretical Assessment of the Mechanism and Site Requirements for Ketonization of Carboxylic Acids on Oxides. *Journal of Catalysis*, **345**, 183-206. https://doi.org/10.1016/j.jcat.2016.11.006

Annex, Scheme 1: Cu(Ac)₂·H₂O Reaction Mechanism of Thermal Decomposition under Air and Ar

$+ 2\ H_2O$

① ②

$2\ Cu + 4\ H_3C\text{-}COOH$

3''

③

④

⑤

$+ 2$

⑤ + 2

Air   Ar

⑥   6 CO_2 + 5 H_2O + 2 CuO

⑥

⑦

⑧

⑩   2 Cu + $\frac{1}{2}$ CO_2 ←   ⑨   2 H_3COOH + Cu_2O + 2 C + 3 H_2